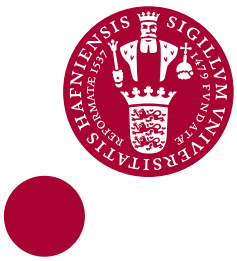

Electric-field controlled spin reversal in a quantum dot with ferromagnetic contacts

Hauptmann, Jonas Rahlf; Paaske, Jens; Lindelof, Poul Erik

Published in:
Nature Physics

DOI:
10.1038/nphys931

Publication date:
2008

Document version
Early version, also known as pre-print

Supplementary material for "Electric-field controlled spin reversal in a quantum dot with ferromagnetic contacts"

J.R. HAUPTMANN[1*], J. PAASKE[1] AND P.E. LINDELOF[1]

[1]The Niels Bohr Institute & The Nano-Science Center, University of Copenhagen, DK-2100 Copenhagen, Denmark

[*]e-mail: rahlf@fys.ku.dk.

(Dated: March 25, 2008)

I. DOMAIN SWITCHING AND STRAY-FIELDS

Magnetic force microscopy images of devices similar to the ones measured, reveal a typical domain-size of $V_{dom} = 100 \times 500 \times 50\, nm^3$, which suggests that the carbon nanotube quantum dot is most likely coupled to one single domain in both source, and drain electrodes. Using the saturation magnetization for Ni, $M_s = 0.61\mathrm{T}/\mu_0$, the magnetic moment of a single contact-domain can be estimated by $V_{dom} M_s$. With 200 nm between the electrodes, this gives a crude estimate of the dipole-dipole interaction energy of the two contact-domains with an energy-gain of roughly 200 eV between the parallel (P) and anti-parallel (AP) configurations. Starting in the P-configuration for a large applied magnetic field, this in turn implies a transition to AP-configuration once the external field becomes smaller than some 30 mT. The switching from P to AP observed in article-figures 2**a,c** occurs at fields smaller than 80 mT for device 1 and close to 60 mT for device 2. Article-figures 2**a,c** were recorded with a resolution in B of 80 mT and 20 mT, respectively. This simple estimate of course neglects all intra-electrode domain-interactions, which cannot a priori be assumed to be less important.

From this we can also estimate the stray-field at the middle between the two electrodes. In the AP-configuration it is close to zero and in the P-configuration it must be roughly $B_{stray} \sim 100\,\mathrm{mT}$, i.e. a factor of 10 and 5, respectively, smaller than the tunneling-induced exchange-fields which we read off from article-figures 2**a,c**. We note that this rather crude estimate is comparable in magnitude to the estimates made in Refs. 1–3. Notice also that stray-fields cannot account for the gate dependence observed in article-figures 3**d-g**.

The fact that the exchange-field cannot be completely compensated by the external field in device 2 is interpreted as a misalignment of $\mathbf{B}_{ex}$ and $\mathbf{B}$. Since bulk Ni has only weak magnetic anisotropy, this is most likely due to the reduced geometry and surface roughness of the electrodes. The fit shown in article-figure 2**d** takes a fixed direction of the magnetization which is found to be $\angle(\mathbf{B}, \mathbf{B}_{ex}) \sim 25^\circ$. We have also tried to make another fit with a finite anisotropy barrier, using a simple Stoner-Wohlfarth model where the magnetic energy of the system is given by

$$E = K \sin^2(\theta - \phi) - BM \cos(\phi), \tag{1}$$

in terms of applied field B and magnetization M at a relative angle ϕ, together with an angle θ between an easy-axis and the applied field. K parameterizes the anisotropy barrier, thus allowing the magnetization to align with $\mathbf{B}$ for large enough values of BM/K. Minimizing

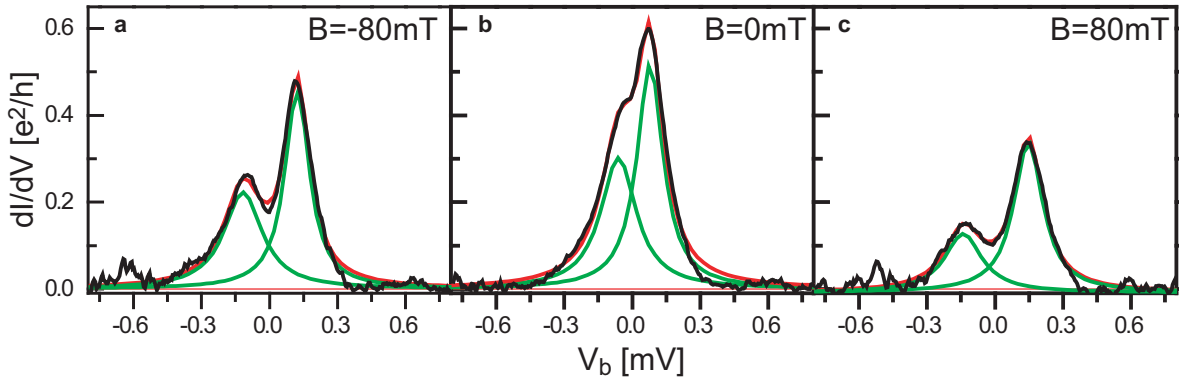

FIG. 1: Plots of dI/dV as a function of bias voltage for $B = -80\,\mathrm{mT}$, $B = 0\,\mathrm{mT}$ and $B = 80\,\mathrm{mT}$ the plots are line-cuts through the plot shown in article-figure 1**a**, measured on device 1. The black curves are the measurements with a baseline subtracted. The green lines are Lorentzian fits to the peaks and the red lines are the resulting double-peak fits. The center-to-center distance of the Lorentzians in each of the three plots gives the splitting of the spin-up and spin-down states on the dot. The splittings are 0.239, 0.139 and 0.287 mV for **a**, **b** and **c**, respectively, corresponding to domain configurations which are **a** parallel, **b** anti-parallel and **c** parallel.

this energy as a function of angle for a given applied field gives a hysteretic magnetization curve from which we can then infer the sum of applied, and exchange-field to determine the spin-splitting as a function of B. Nevertheless, this fit performed no better than the far simpler fit to a fixed angle.

II. ADDITIONAL PLOTS FOR DEVICES 1 AND 2

A. Device 1

The ratio of the couplings to respectively source and drain electrodes can be estimated from the formula

$$\frac{\Gamma_s}{\Gamma_d} = \frac{\Delta V_P - 2g\mu_B B/e + \Delta V_{AP}}{\Delta V_P - 2g\mu_B B/e - \Delta V_{AP}}, \tag{2}$$

where $V_P(V_{AP})$ denotes the splittings in the parallel (antiparallel) configuration which are read off from figure 1. This gives the estimate $\Gamma_s/\Gamma_d \sim 3$, cited in the main paper.

The plots in figure 2 shows the differential conduction as a function of gate and bias voltage measured at different magnetic fields. The measurements are made on device 1 after

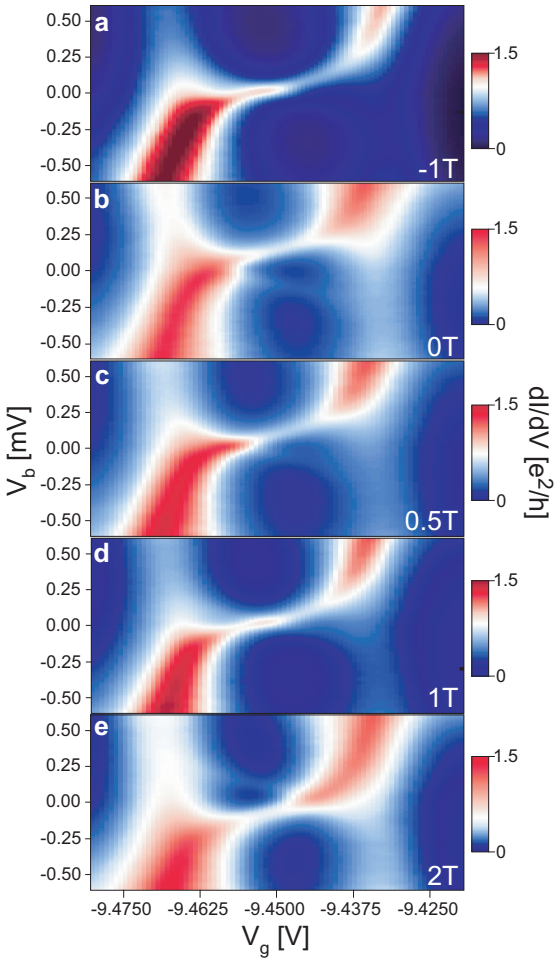

FIG. 2: Gate-dependence of the spin-states probed by the split Kondo-peak measured on device 1 post switch. **a-e** show the differential conductance as a function of gate, and bias-voltage measured at different magnetic fields. Notice that the crossings of the Kondo ridges move to the right as the magnetic field is increased. It is from these plots the scatters and the fits in article-figure 4 **a** is made.

a switch, i.e. a sudden, permanent change in the device behavior. Notice that the crossing of the Kondo ridges moves from left to right as the magnetic field is increased. It is these measurements that the scatter and fits in article-figure 4**a** are made from. Note that the plot measured at $B = -1\,\mathrm{T}$ has also been fitted but is not shown in article-figure 4**a** since it is placed right on top of $B = 1\,\mathrm{T}$. The plot made at $B = 0\,\mathrm{T}$ is not included in the fitting since the domain configuration is expected to be different. The point corresponding to $B = 1\,\mathrm{T}$ in the inset of article-figure 4**a** is really the average of the fitted constants, 0.065 mV and 0.053 mV, obtained at $B = -1\,\mathrm{T}$ and $B = 1\,\mathrm{T}$, respectively.

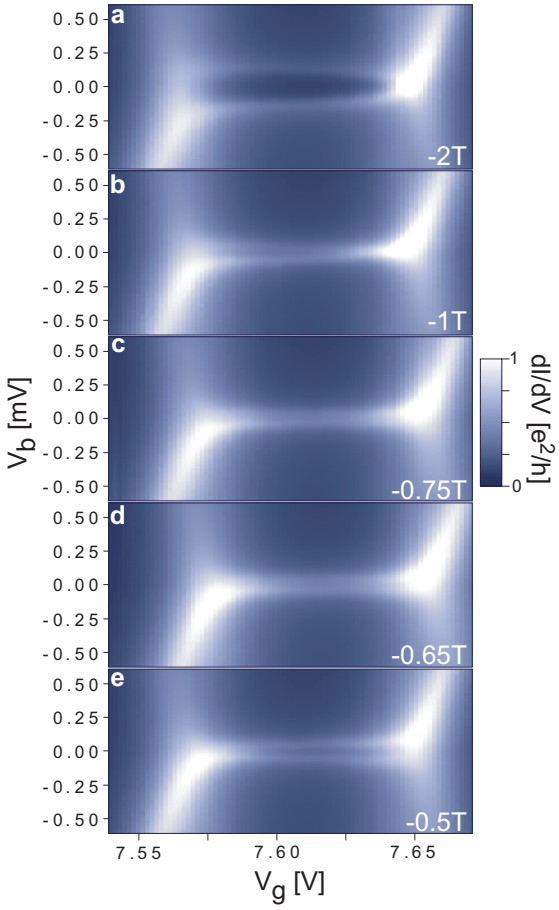

FIG. 3: Gate dependence of the spin-states probed by the Kondo effect measured on device 2. **a-e** show the differential conduction as a function of gate and bias voltage measured at different magnetic fields. Notice that the Kondo ridges do not cross in any of the plots. This is interpreted as a misalignment of the domains and the external field.

B. Device 2

The plot shown in figure 3 shows the differential conductance as a function of gate, and bias voltage measured at different magnetic fields. The slopes of the Kondo ridges in **a, b** and in **e** are clearly opposite, although the measurements at intermediate magnetic fields (**c, d**) show no crossing of the Kondo ridges. We ascribe this to a misalignment of the domain magnetization direction (and therefore the exchange field) and the external magnetic field.

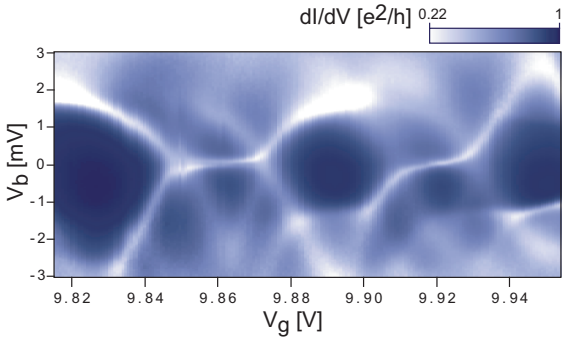

FIG. 4: Five Coulomb diamonds with a Kondo resonance in every second. The plot show the differential conduction as a function of gate and bias voltage.

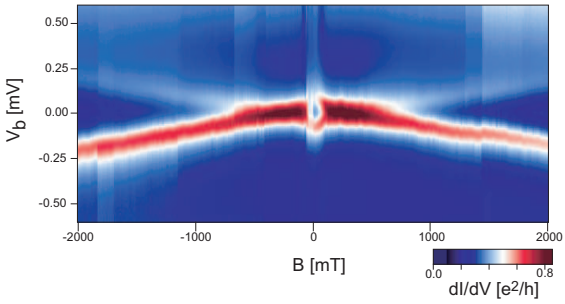

FIG. 5: Kondo peak splitting as a function of magnetic field at fixed gate voltage measured on device 3. The plots shows the differential conduction as a function of bias and magnetic field, swept from 2 T to -2 T.

III. PLOTS FOR DEVICES 3 AND 4

Figure 4 shows the differential conduction as a function of gate, and bias voltage. Two Kondo ridges near zero bias can be observed and henceforth we shall refer to the corresponding odd-numbered Coulomb-blockade diamonds as devices 3 and 4, respectively. These measurements are made on the same physical device as device 1 but off-set in gate voltage by roughly 20 V. Note that devices 1 and 2 are measured on two different physical devices sharing an electrode and the back-gate.

Figure 5 shows dI/dV as a function of bias voltage and magnetic field. The measurements are made close to the middle of the Coulomb-blockade diamond in device 3. A linear splitting of the Kondo peak with magnetic field can be observed, as would be expected since this device should be contacted by the same domains as device 1 and the domain configuration

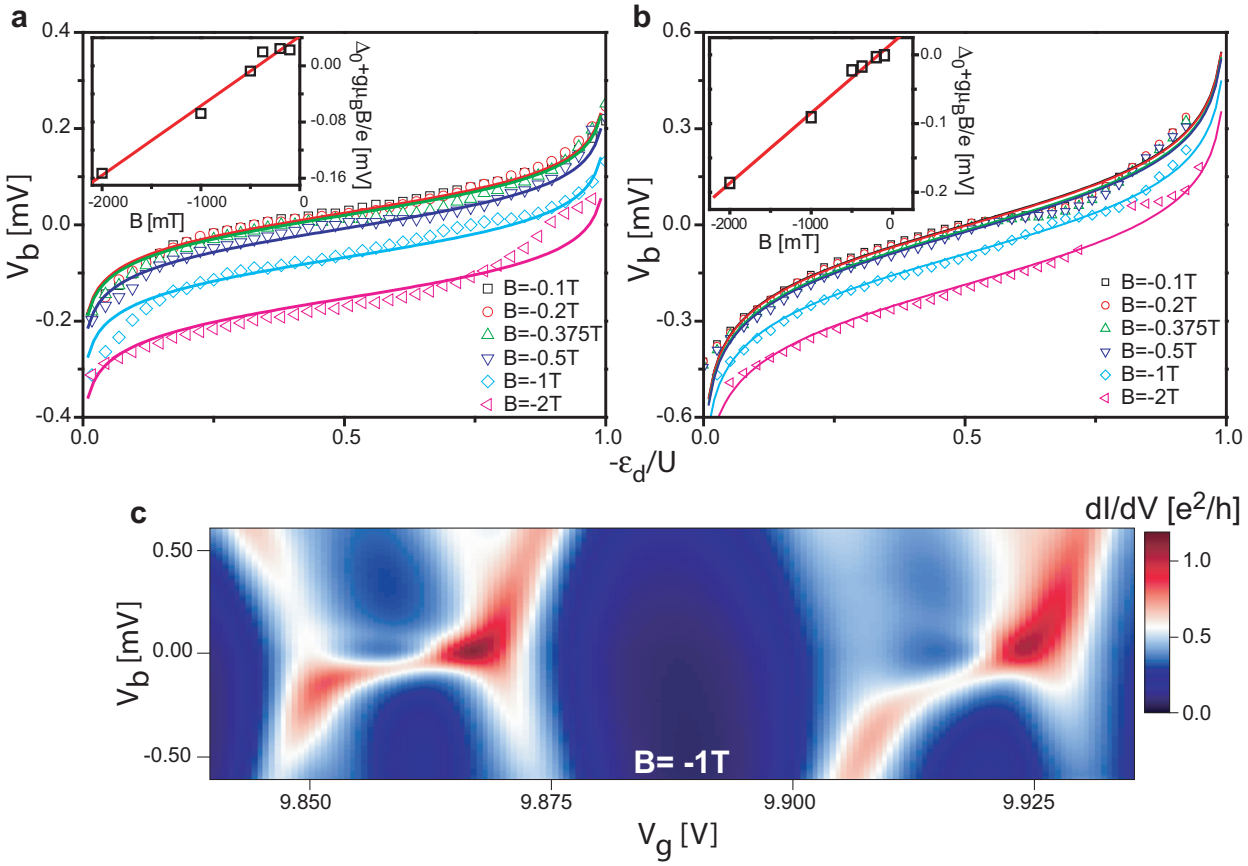

FIG. 6: Gate dependence of the exchange field for different applied magnetic fields measured on **a** device 3 and **b** device 4. **c** Show the differential conduction as a function of bias and gate voltage the measurement are made with an external field of -1 T. Four Coulomb peaks and two Kondo resonances are observed the 1st resonance corresponds to device 3 and the 2nd to device 4. **a, b** shows the scatter plot of the peak position read off from measurement like the one shown in **c**, where the gate voltage have been normalized with the charging energy. The different colors and shapes corresponds to different external magnetic fields. The lines are fits to the scatters. The insert shows the fitting constant $\Delta_0 + g\mu_B B/e$ for the different magnetic fields and a linear fit to these points.

and magnetization direction in the electrodes should be independent of the gate voltage.

Figure 6**c** shows a zoom-in on the Kondo ridges, measured at $B = -1$ T. A gate dependent splitting of the Kondo resonance is clearly observed in both device. The different slopes indicate a change in $\Gamma = \Gamma_s + \Gamma_d$ from one Kondo resonance to the next, most likely due to a difference in couplings to the two orbitals in the CNT.

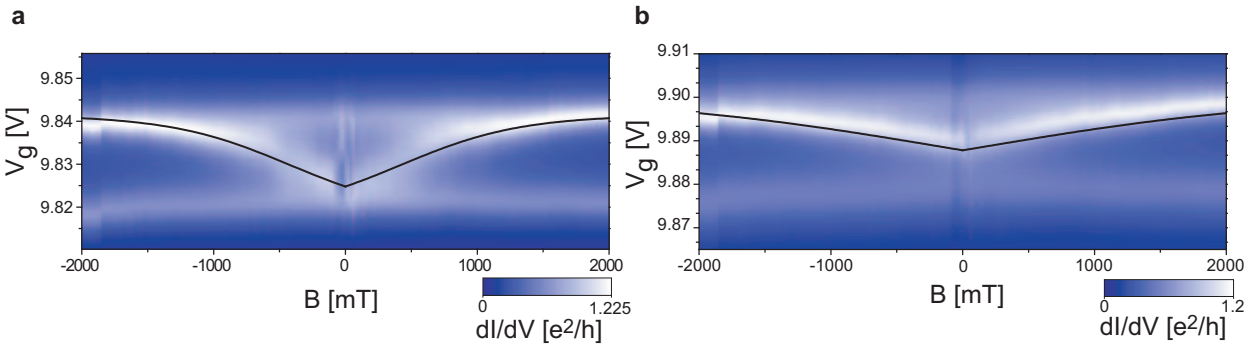

FIG. 7: Gate dependence of the exchange field at zero bias. The plots shows the differential conduction as a function of gate voltage and external magnetic field for device 3 **a** and device 4 **b**. The two horizontal lines in each plot are due to Coulomb peaks. The white line crossing from one peak to the other **a** or halfway between them **b** maps out the Kondo peak movement (the point where the spin states are degenerate) as a function of magnetic field. The black line is a parameter free fit where the constant have been found from the fits in figure 6. Similar to the parameter free fit shown in article-figure 4**b**.

The splittings of the Kondo peaks have been read off and plotted in figure 6**a,b**. The lines are fits to the scatter-plots and the different colors correspond to different external magnetic fields. The fitted values used for $P\Gamma/\pi$ are 0.045 and 0.117 meV for the groups of fits in **a** and **b**, respectively. The insets in both figures show $\Delta_0 + g\mu_B B/e$ as function of B. The two linear fits yield a slope of 9.9×10^{-5} (**a**) and 1.0×10^{-4} (**b**), corresponding to a g-factor of 1.7 and 1.8, respectively.

Figure 7 shows dI/dV as function of gate voltage and magnetic field. Panels **a** and **b** correspond to devices 3 and 4, respectively. The black line is plotted using the procedure described in the caption of article-figure 4**b**, now with parameters obtained from figure 6.

---

[1] Patsupathy, A. N. *et al.* The Kondo effect in the presence of ferromagnetism. *Science* **306**, 86 (2004).

[2] Sahoo, S. *et al.* Electric field control of spin transport. *Nature Physics* **1**, 99 (2005).

[3] Meier, L., Salis, G., Ellenberger, C., Ensslin, K., Gini, E. Stray-field-induced modification of coherent spin dynamics. *Appl. Phys. Lett.* **88**, 172501 (2006).